arXiv:1606.02146v1 [physics.ins-det] 7 Jun 2016

# Low energy recoil detection with a spherical proportional counter

I.Savvidis[a], I.Katsioulas[a,b,*], C.Eleftheriadis[a], I.Giomataris[b], T.Papaevangellou[b]

[a] *Aristotle University of Thessaloniki, Greece*
[b] *IRFU, Centre d'Etudes de Saclay, Gif sur Yvette Cedex, France*

**Abstract**

We present low energy recoil detection results in the keV energy region, from measurements performed with the Spherical Proportional Counter (SPC). An $^{241}Am - {}^{9}Be$ fast neutron source is used in order to obtain neutron-nucleus elastic scattering events inside the gaseous volume of the detector. The detector performance in the $keV$ energy region was resolved by observing the 5.9 $keV$ line of a $^{55}Fe$ X-ray source, with energy resolution of 9% ($\sigma$). The toolkit GEANT4 was used to simulate the irradiation of the detector by an $^{241}Am - {}^{9}Be$ source, while SRIM was used to calculate the Ionization Quenching Factor (IQF). The GEANT4 simulated energy deposition spectrum in addition with the SRIM calculated quenching factor provide valuable insight to the experimental results. The performance of the SPC in low energy recoil detection makes the detector a good candidate for a wide range of applications, including Supernova or reactor neutrino detection and Dark Matter (WIMP) searches (via coherent elastic scattering).

*Keywords:* nuclear recoil detection, WIMP detection, neutrino detection, spherical proportional counter, quenching factor

*Corresponding author
*Email address:* ikatsi@physics.auth.gr (I.Katsioulas)

## 1. Introduction

The detection of very low energy nuclear recoils is essential to the field of direct neutrino detection and of direct dark matter searches. During the last years the dark matter hunt is continued with increasing rate. Weakly Interacting Massive Particles (WIMPs) are an eminent candidate for Dark Matter (DM). A common way of search for this type of particles relies on the elastic scattering of WIMPs on the target nuclei. The recoil energy is expected to be in the $keV$ (or less) energy range, for WIMPs with a mass lower than 10 GeV. Another important field of searches concomitant to that of DM searches [1] (being also a background source to them), is the direct detection of low energy neutrinos ($1\ MeV - 100\ MeV$). Supernova neutrinos, solar, geoneutrinos and reactor neutrinos all belong to this category. The Standard Model neutrino-nucleon interaction was proposed years ago and it is gaining in popularity lately, because of the large cross section it provides through the coherence effect, where all nucleons contribute to the scattering (especially the neutrons), resulting in a cross section increased by the neutron number squared. Again the detection of these neutrinos relies on the observation of the recoiling nuclei in the $keV$ energy range and depending on the neutrino source, observing recoils of a few hundred $eV$ (reactor neutrinos for example [2, 3]). These applications require a detector with a very low detection energy threshold ($\sim\ 100\ eV$). We propose the utilization of the SPC, a spherical gaseous detector, recently developed by Giomataris et al [4], for applications with such requirements. In this work, we present the low energy detection capabilities of the SPC, as well as the simulated detector response to low energy recoils, taking into account the effect of the Ionization Quenching Factor (IQF) [5] by using GEANT4 [6] and SRIM [7].

## 2. The spherical proportional counter

The detector consists of a spherical vessel which is grounded and filled with a gas mixture (up to 5 *bar* pressure). The anode which consists of a small ball

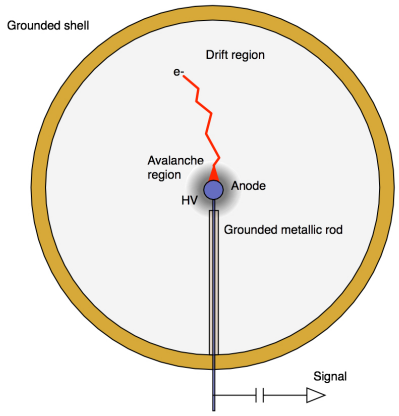


Figure 1: A schematic of the Spherical Proportional Counter and the detection principle.

(usually made from a metallic or a resistive material), is placed in the center of the vessel and supported by a grounded metallic rod, through which the high voltage is applied. Thus the electric field is varying with the reverse of the distance squared ($1/r^2$) and it is highly inhomogeneous along the radius. The difference in the intensity of the electric field, from the outer to the inner radii, divides the detector volume into two regions, the drift and the amplification region (figure 1). Primary ionization electrons in the drift region, drift towards the anode (the drift time varies from $us$ to $ms$ depending on the gas mixture and pressure). When these electrons reach a distance of a few mm from the anode, the avalanche starts due to the intense electric field. The induced signal passes through a charge sensitive preamplifier, read-out by an Analog to Digital Converter (ADC) and registered to a computer memory. The pulse shape of the signal, depends on the charge spatial density distribution and the distance of the interaction from the anode. The main advantages of this detector, for low energy recoil detection (either neutrino or WIMP induced recoils), are the simple design, the large volumes achievable, the energy resolution in the low energy region ($< 10\%$ at 5.9 $keV$) [8, 9] and the low electronic noise provided by the low capacitance due to the spherical geometry [10] (even for large detector sizes).

The low energy threshold of the detector is limited only by the mean ionization energy of the gas mixture [8]. The detection range varies from a few $eV$ to tenths of $MeV$, depending on the amplification field, allowing detection of low energy gammas, electrons, alpha particles and heavy ions. Lastly, the fiducialization capability of the detector, allows us to distinguish point like energy depositions (low energy gammas, low energy electrons, heavy ions), from spatially extended depositions (muons), through pulse shape analysis. A complete description of the SPC (principle of detection, characteristics and capabilities) can be found at [4].

## 3. Experimental set up and low energy calibration

A SPC placed at the Aristotle University of Thessaloniki, was used for this study. The spherical vessel of the detector is 40 $cm$ in diameter and made from 1.5 $cm$ thick Duran 2.3 glass (coated with a graphite layer). The anode in the center of the cavity is metallic, 2 $mm$ in diameter. The vessel was filled with $Ar : CH_4$ 98 : 2 gas mixture at different pressures. The low energy calibration of the detector was performed using a $^{55}Fe$ source (5.9 $keV$) and the fluorescence lines of $^{27}Al$ (1.45 $keV$) [9] and $^{241}Am$ (13.95 $keV$, 17.7 $keV$) [11]. To test the response of the detectors to neutrinos or WIMPs, nuclear recoils have to be produced, for this reason the detectors were exposed to an $^{241}Am - ^{9}Be$ source with an activity of $5.94 \times 10^4$ neutrons per second (figure 3). The $^{241}Am - ^{9}Be$ source also emits gamma rays, the most important line being the 4.44 MeV line from the deexcitation of the $^{12}C^*$ nucleus, produced from the $Be(\alpha, n)$ reaction [12]. The intensity of this line is directly related to that of the neutron intensity, with a ratio $R = S_g/S_n = 0.591 \pm$ 2.6% [13].

The source was placed 15 $cm$ away from the surface of the detector. To prevent gamma ray contamination, it was cased inside a lead castle of 12 $cm$ thickness along the axis. The effect of the shielding to the neutron spectrum and the 4.44 $MeV$ line was simulated using GEANT4. The neutron spectrum that enters the gaseous volume, along with the gamma ray spectrum coming from

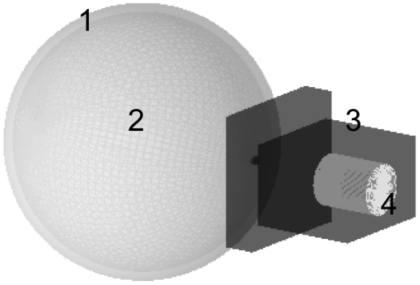


Figure 2: A schematic of the detector setup: 1) The detector vessel, 2) the gaseous volume, 3) the lead shielding and 4) the source case.

the interaction of the neutrons with the surrounding materials is presented at figure 3. More on the simulations will be discussed at Section 5.

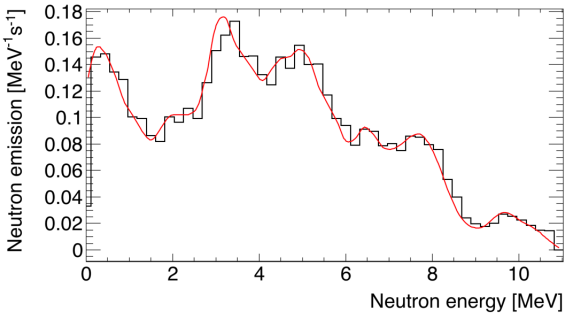


Figure 3: The simulated $^{241}Am - {}^{9}Be$ neutron emission spectrum (black) and the ISO 8529 [14] neutron emission spectrum (red).

## 4. Results – Pulse shape analysis

The detector was filled with $Ar : CH_4$ 98 : 2 at 500 $mbar$ and was irradiated by the $^{241}Am - {}^{9}Be$ source; due to cosmic radiation (ie atmospheric muons [15] and neutrons) and natural radioactivity from the surrounding walls (ie $^{40}K$, $^{238}U$ and $^{232}Th$ daughter isotopes) the background contribution had to be measured also, in order to be subtracted from the recorded signal. The data acquired were analyzed using Pulse Shape Analysis (PSA). The parameters used

in the analysis were a) the pulse amplitude (pulse maximum), b) the pulse rise time (time interval between 10% and 90% of the pulse height) c) the Full Width at Half Maximum (FWHM) of the pulse. Figures 4, 5 and 6 show the results of the analysis without any pulse shape cuts. The atmospheric muon contribution to the energy deposition spectra is visible at figure 4 (top diagram) as a "peak" with energy around 20 $keV$.

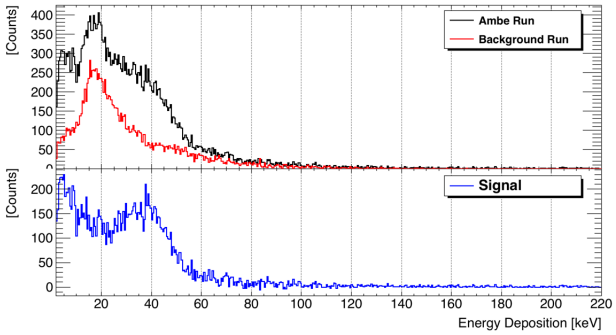


Figure 4: Top diagram: energy deposition spectra of the $^{241}Am - ^{9}Be$ run (black line) and the background (red line). Bottom: difference between the two. No cuts are applied.

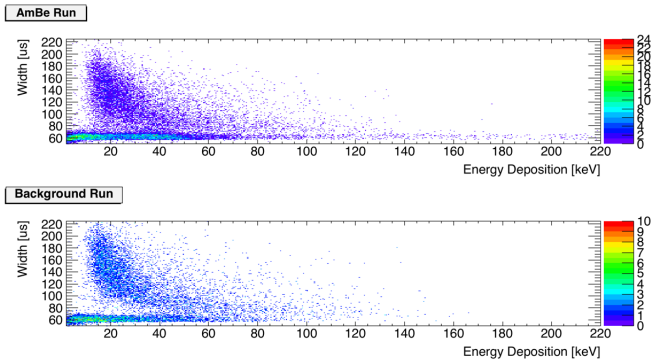


Figure 5: The width of the pulse versus energy deposition for the $^{241}Am - ^{9}Be$ run (top) and the background run (bottom), without any cuts.

Atmospheric muons cross the whole length of the detector volume, depositing energy along their long track ($\sim$ tenths of $cm$). They can also produce delta rays, energetic enough to ionize further at a distance from the primary track,

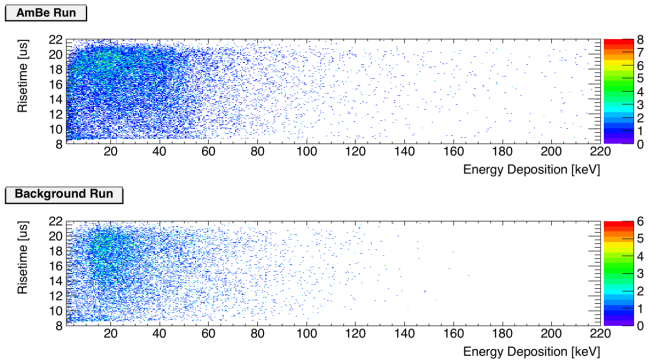


Figure 6: The pulse rise time versus energy deposition for the $^{241}Am - {}^{9}Be$ run (top) and the background run (bottom), without any cuts.

creating ionization clusters with large charge density. This kind of "behavior" is translated to pulses with higher width (than punctual depositions), which may contain multiple peaks (due to variations in drift time and in spatial ionization density), as for example the pulse presented in figure 7. In figure 8 the number of peaks per event versus the energy deposition is presented for the $^{241}Am - {}^{9}Be$ run.

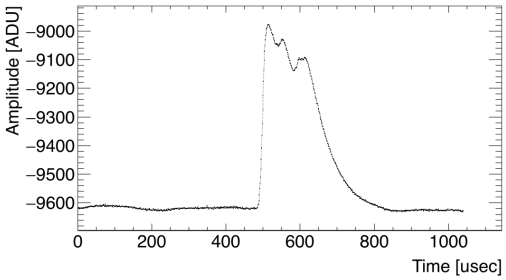


Figure 7: Example of a muon induced pulse displaying double peak.

To minimize the muon contribution, we selected events with: pulse width values between 50 $us$ and 70 $us$, pulse rise time values between 11 $us$ and 21 $us$ and events with only one peak. The final results after cutting off the muon induced events are presented in figures 9, 10 and 11.

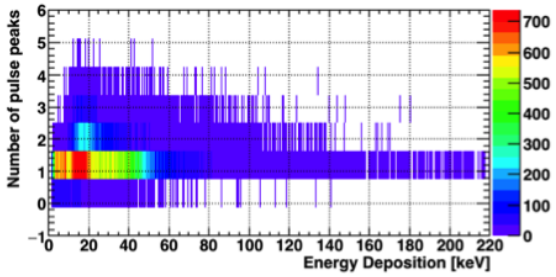


Figure 8: The number of peaks versus the energy deposition per event, for the $^{241}Am - ^{9}Be$ run.

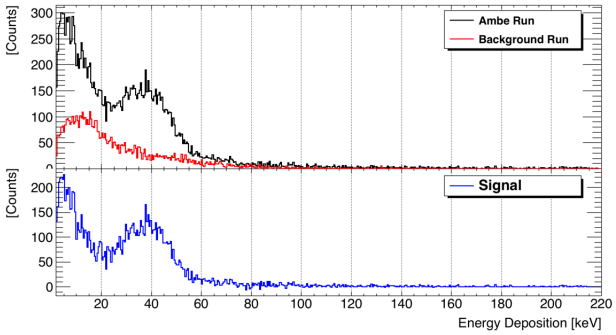


Figure 9: Top diagram: energy deposition spectra of the $^{241}Am - ^{9}Be$ run (black) and the background (red). Bottom: difference between the two (blue). The results are shown after the muon cuts.

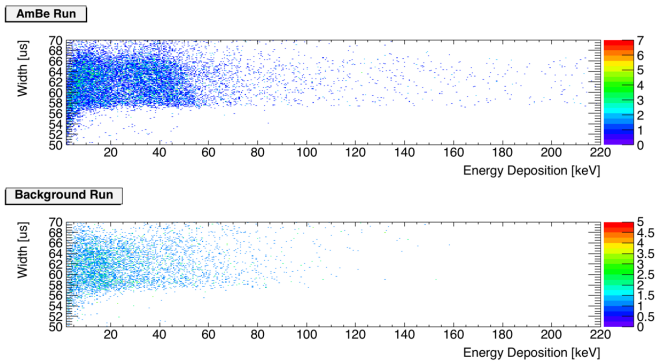


Figure 10: The width of the pulse versus energy deposition of the pulse histograms for the $^{241}Am - ^{9}Be$ run (top) and the background (bottom), after applying the muon pulse shape cuts.

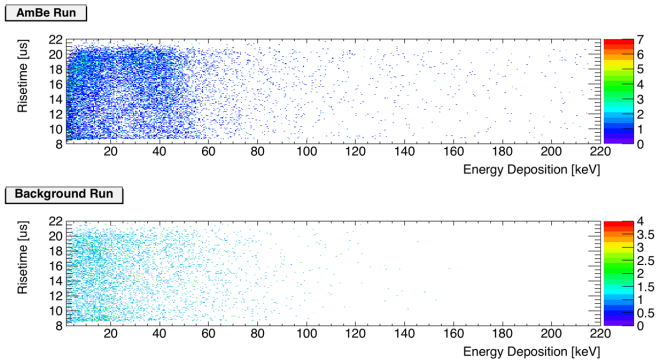


Figure 11: The pulse rise time versus energy deposition for the $^{241}Am - ^{9}Be$ run (top) and the background (bottom), after applying the muon cuts.

## 5. Simulations – Comparison with experimental results

### *5.1. The GEANT4 simulation*

The exact experimental configuration, was simulated by using GEANT4 [6]. Figure 3 shows the simulated neutron emission spectrum from the $^{241}Am - ^{9}Be$ source compared with the reference emission spectrum ISO8529 [14]. The "`FTFP_BERT_HP_LIV`" physics list was chosen in the simulation to include the high precision transport model [16], for neutrons with energy lower than 20 $MeV$ and also to include the "Livermore" model [17] for a more detailed description of the low energy electromagnetic interactions ($\sim$ $keV$). The number of neutron, electron and gamma particles that enter into the gaseous volume of the detector was calculated as shown in figure 12.

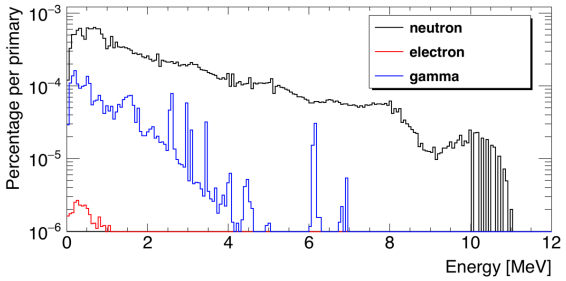


Figure 12: The simulated number of electron, neutron and gamma particles that enter to the detector volume per primary neutron.

The energy deposited by these particles in the detector volume, taking into account all the different physics processes that they undergo is shown in figure 13. The contribution from all particles forms the total energy deposition spectrum. The GEANT4 simulation output for the energy deposition of the low energy ions represents the total kinetic energy dissipated inside the medium but there is no differentiation between energy spend on ionization or excitation of the medium and on "nuclear" energy losses. For this reason the quenching factor has to be taken into account.

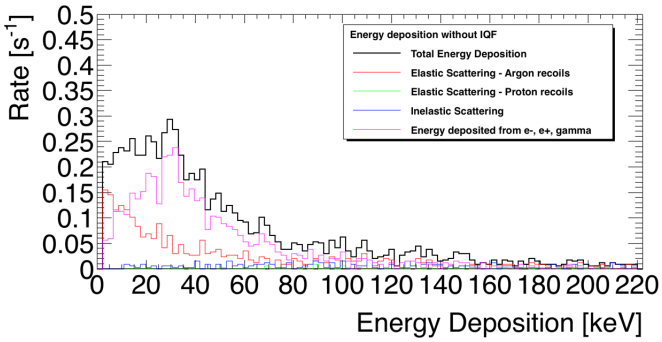


Figure 13: The energy deposition spectra from the different energy depositing particles coming from the neutron emission of the $^{241}Am - ^{9}Be$ source, without considering the ionization quenching factor.

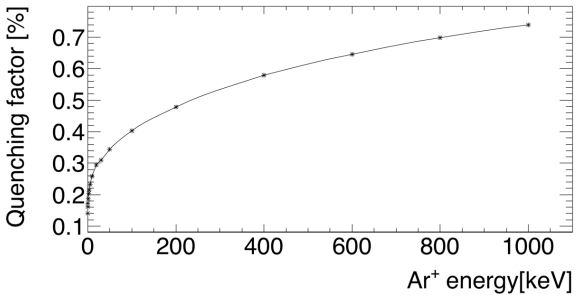


Figure 14: The ionization quenching factor for $Ar : CH_4$ 98 : 2 gas mixture calculated using SRIM.

### *5.2. SRIM simulation of the Ionization Quenching Factor (IQF)*

Ionization quenching factor is defined as the fraction of the kinetic energy of an ion that is dissipated in a medium in the form of ionization electrons and excitation of the atomic and quasi-molecular states [18]. The quenching factor is directly related to the stopping power of matter for ions. The energy loss of ions was estimated by the work of Lindhard et al [19]. The stopping power can be divided into the electronic stopping power $S_e$ and the nuclear stopping power $S_n$, which is due to elastic scattering of ions on atoms. Together they give us the total stopping power of a medium. For high energy ions the total stopping

power is dominated by the electronic energy losses, as the nuclear stopping is negligible [5]. When the ion energy decreases the importance of the nuclear scattering increases and the nuclear stopping power $S_n$ becomes of the same order of magnitude as the electronic stopping power $S_e$. For ions with velocity lower than the Bohr orbital speed of atomic electrons ($v_{ion} \leq v = e^2/\hbar = c/137$) [20] the nuclear stopping becomes predominant. The knowledge of the quenching factor is of paramount importance to the direct detection of coherent neutrino interactions and WIMPs since the detection of these particles, relies on the detection of low energy nuclear recoils, produced after the elastic scattering on target nuclei. There have been many efforts to measure the quenching factor in different materials, but few results have been published due to the very low energy detection threshold required. The quenching factor besides the Lindhard theory can also be estimated with other means such as the SRIM [7]. Such calculations have been done before [21] and are in agreement with experimental measurements. The quenching factor estimation for the $Ar : CH_4$ 98 : 2 gas mixture as a function of the $Ar^+$ ion energy is presented in figure 14.

Taking into account the IQF, the GEANT4 simulated energy deposition by low energy ions (figure 15), was altered to correspond to the electromagnetic energy losses ($S_e$). In addition the source gamma emission contribution was simulated [11] and the results are presented in figure 16. Comparing the data (figure 9-bottom) with the simulations, the main contributions in the energy deposition spectrum are explained. The low energy area up to 20 $keV$ is due to the energy deposited by the elastically scattered ions and the peak with center at $\sim 35$ $keV$ is mainly due to the gamma rays emitted by the interaction of the source neutrons with the detector materials.

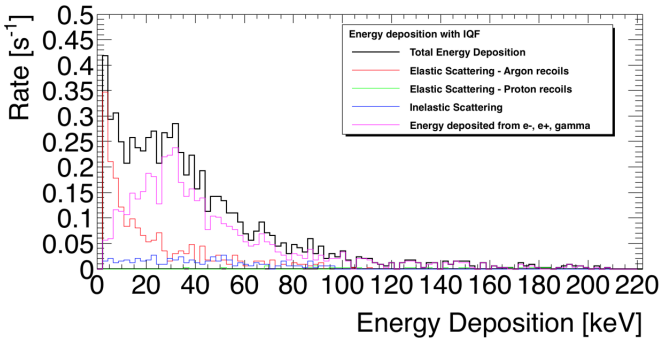


Figure 15: The energy deposition spectra from the different energy depositing particles coming from the neutrons emitted by the $^{241}Am - ^{9}Be$ source with the detector materials, taking into account the ionization quenching factor.

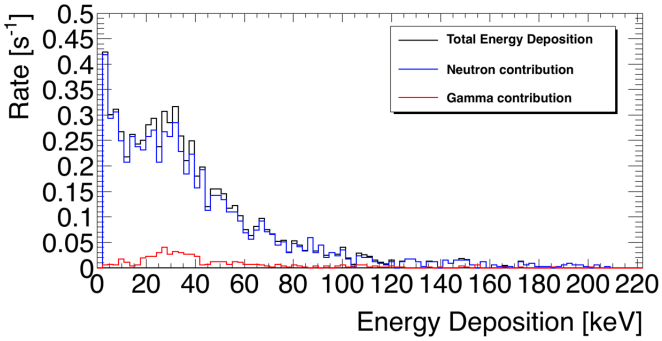


Figure 16: The total energy deposition (taking into account the IQF) from the neutron emission component and the gamma emission component of the $^{241}Am - ^{9}Be$ source.

## 6. Conclusions

The SPC is capable of detecting very low energy nuclear recoils (in the few $keV$ energy region), thus being a very good candidate for rare event searches. The results of the GEANT4 simulations in combination with IQF calculation by using SRIM are in good agreement with the results from the PSA of the data taken. For the future we plan to increase the pressure of the gas mixture up to 5 $bar$ and try to detect heavy recoils at energies below 1 $keV$ (ultra low energy recoil detection). We also would like to perform background studies to improve

the recoil to background events ratio.

## Acknowledgments

This research/publication has been co-financed by the European Union (European Social Fund ESF) and Greek national funds through the Operational Program "Education and Lifelong Learning" of the National Strategic Reference Framework (NSRF) - Research Funding Program: THALIS HELLENIC OPEN UNIVERSITY- Development and Applications of Novel Instrumentation and Experimental Methods in Astroparticle Physics.

## References

[1] Gerbier G. et al arXiv:{1401.7902}.

[2] J. D. Vergados, Journal of Physics: Conference Series 309 (1) (2011) 012031.

[3] Tsakstara, V., Kosmas, T. S, Phys. Rev. C 84 (2011) 064620. doi:10.1103/PhysRevC.84.064620.

[4] Giomataris, I. et al, JINST 3 (2008) P09007. arXiv:0807.2802, doi:10.1088/1748-0221/3/09/P09007.

[5] Hitachi, A., J. Phys. Conf. Ser. 65 (2007) 012013. doi:10.1088/1742-6596/65/1/012013.

[6] Agostinelli, S. et al, Nucl. Instrum. Meth. A506 (2003) 250–303. doi:10.1016/S0168-9002(03)01368-8.

[7] Ziegler, J. et al, Nuclear Instruments and Methods in Physics Research B 268 (2010) 1818–1823. doi:{10.1016/j.nimb.2010.02.091}.

[8] Bougamont, E. et al, J. Phys. Conf. Ser. 309 (2011) 012023. doi:10.1088/1742-6596/309/1/012023.

[9] Bougamont, E. et al arXiv:{1010.4132}.

[10] Andriamonje, S. et al, J. Phys. Conf. Ser. 179 (2009) 012003. doi:10.1088/1742-6596/179/1/012003.

[11] Zhenzhou, L. et al, Applied Radiation and Isotopes 65 (12) (2007) 1318 – 1321. doi:http://dx.doi.org/10.1016/j.apradiso.2007.04.007.

[12] Mowlavi, A., Koohi-Fayegh, R., Applied Radiation and Isotopes 60 (6) (2004) 959 – 962. doi:http://dx.doi.org/10.1016/j.apradiso.2004.02.008.

[13] A. Croft, Nuclear Instruments and Methods in Physics Research Section A: Accelerators, Spectrometers, Detectors and Associated Equipment 281 (1) (1989) 103 – 116. doi:http://dx.doi.org/10.1016/0168-9002(89)91221-7.

[14] ISO 8529-1, International Organization for Standardization, Geneva, Switzerland (2001).

[15] P. Grieder, Cosmic Rays at Earth, Elsevier Science, 2001.

[16] G. Collaboration, Physics reference manual.
URL http://geant4.web.cern.ch/geant4/G4UsersDocuments/UsersGuides/PhysicsReferenceManual/html/PhysicsReferenceManual.html

[17] G. Cirrone, G. Cuttone, F. D. Rosa, L. Pandola, F. Romano, Q. Zhang, Validation of the geant4 electromagnetic photon cross-sections for elements and compounds, Nuclear Instruments and Methods in Physics Research Section A: Accelerators, Spectrometers, Detectors and Associated Equipment 618 (13) (2010) 315 – 322. doi:http://dx.doi.org/10.1016/j.nima.2010.02.112.

[18] Platzman, R.L., The International Journal of Applied Radiation and Isotopes 10 (23) (1961) 116 – 127. doi:http://dx.doi.org/10.1016/0020-708X(61)90108-9.

[19] Lindhard, J. et al, Mat. Fys. Medd. K. Dan. Vidensk. Selsk. 33.

[20] R. Evans, The Atomic Nucleus, McGraw-Hill, 1955.

[21] Santos, D. et al `arXiv:{0810.1137}`.